International Journal of Modern Physics E
Vol. 27, No. 3 (2018) 1850026 (22 pages)

DOI: 10.1142/S021830131850026X

World Scientific
www.worldscientific.com

Features about pion production in 2.1A and 3.7A GeV ^{4}He–nucleus interactions up to and out of kinematical limit

A. Abdelsalam*,†, B. M. Badawy†,‡,¶, H. A. Amer§, W. Osman*,†, M. M. El-Ashmawy§ and N. Abdallah†,§

*Physics Department, Faculty of Science, Cairo University, Giza, Egypt

†Mohammad El–Nadi High Energy Lab, Faculty of Science, Cairo University, Egypt

‡Reactor Physics Department, Nuclear Research Center, Atomic Energy Authority, Egypt

§Nuclear and Radiological Regulatory Authority, NRRA, Egypt

¶he_cairo@yahoo.com

Received 14 October 2017
Revised 22 February 2018
Accepted 22 February 2018
Published 21 March 2018

The shower particle multiplicity characteristics are studied in 2.1A and 3.7A GeV ^{4}He interactions with emulsion nuclei. The dependencies on emission direction, energy, target size, and centrality are examined. The data are compared with the simulation of the modified FRITIOF model. The forward emitted pion multiplicity distributions exhibit KNO scaling. The decay or peaking shaped curves characterize the pion multiplicity distributions. The decay shape is suggested to be due to a single source contribution and the peaking one results from a multisource superposition. The forward emitted pion is created from fireball or hadronic matter. The target nucleus is the origin of the backward one, regarding the nuclear limiting fragmentation hypothesis.

Keywords: Pion source; forward–backward emission; modified FRITIOF model.

PACS Number(s): 25.75.−q, 25.75.Dw, 25.75.Gz, 25.75.Ld, 25.70.Mn, 25.70.Pq, 41.75.Ak, 41.75.Cn, 29.40.Rg, 07.68.+m

1. Introduction

In high-energy nuclear collision, the two nuclei can overlap according to the impact parameter. The nucleons in the overlap region are the participants. The projectile participant nucleon strikes one or several target nucleons in, the binary nucleon–nucleon (NN) collisions and intranuclear cascading. In the overlap volume, a hot and dense fireball develops.[1,2] If the fireball temperature or density becomes larger than critical values, quark–gluon plasma (QGP) can be created. The fireball begins to expand and cool, after which the QGP hadronizes to form a large number of

hadrons. Most of the produced pions are the final decay of these hadrons. The hadronization can be treated in the light of the Lund string model,[3] which is used in the Monte Carlo FRITIOF model.[4–6] In the few GeV region, the particles are produced on the basis of the binary NN collisions as; $NN \rightarrow N\Delta$ picture. After the decay of the resonance, the meson is produced. In ultrarelativistic region, say SPS energies, the hadron is produced due to the formation of quantum chromo dynamic string. Kinematically the hadron flies into the forward hemisphere (FHS). The emission in the backward hemisphere (BHS) is beyond the kinematic limits. It was studied for the first time at Dubna and Lawrence Berkeley National Laboratory (LBNL).[7–11] It was suggested that the backward emitted pion is a target source particle.[8,12,13] The available space angle of the emitted particle can be identified by the FRITIOF model.[6] In the original FRITIOF model the Glauber-like approximation provides inadequate amount of intranuclear cascading. As a result, some difficulties were found to predict the nuclear fragmentation and the pionization at few GeV energies. These difficulties were overcome by Reggeon theory which provides sufficient amount of intranuclear cascading. The simulation at large emission angles of the pion could be improved also by coupling the FRITIOF model with the binary cascade model.[14] Modifying the original FRITIOF model by the Reggeon theory resulted in the, so-called modified FRITIOF model (MFM).[6,15–17]

The pion production has been recently studied at the LHC energies by ALICE collaboration.[18,19] It has been of interest in Brookhaven National Laboratory (BNL) by PHENIX,[20–22] BRAHMS,[23] and STAR[24–27] collaborations at RHIC energies. Pion production studies were also carried out by our lab group.[12,13,28–39] In the photographic nuclear emulsion nomenclature, the major fraction of the produced shower particles (more than 90%) are charged pions.[36,40–42] In this experiment, the shower particles are used as a tool to study the pion production. They are classified into two groups according to the emission zone in the 4π space. One encloses those emitted in the FHS at $\theta_{\rm lab} < 90^\circ$. The other encloses those emitted in the BHS at $\theta_{\rm lab} \geq 90^\circ$. The present interactions are 2.1A and 3.7A GeV ^{4}He with emulsion nuclei. Nuclear emulsion, as a target, provides a wide range of nuclear size ($A_T = 1$ up to 108). The shower particle multiplicity characteristics are determined at average impact parameter and different centralities. At average impact parameter the data sample is unbiased to any centrality criteria and selected randomly. The simulation code used in this work is the modified FRITIOF model (MFM). This modification was carried out by V. V. Uzhinskii, LIT, JINR, Dubna, Russia, based on the original FRITIOF version 1.6.[4,5]

2. Experimental Details

2.1. *Nuclear emulsion*

In the present experiment, two stacks of NIKFI–BR2 emulsion are irradiated by 2.1A and 3.7A GeV ^{4}He at the Synchrophasotron, JINR, Dubna, Russia. The

Table 1. Atomic density of the NIKFI–BR2 emulsion.

Element	^{1}H	^{12}C	^{14}N	^{16}O	^{80}Br	^{108}Ag
$\rho \times 10^{22}\,\mathrm{cm}^{-3}$	3.150	1.410	0.395	0.956	1.028	1.028

dimensions of each pellicle in the stack are 20 cm × 10 cm × 0.06 cm. The atomic density (ρ) of each constituent emulsion element is listed in Table 1.

2.2. *Particle identity*

The tracks can be identified in the photographic nuclear emulsion according to the common terminology[41,42] as:

— Shower particle: It is a track having $g \leq 1.4g_p$, where g is the measured grain density and g_p corresponds to the grain density of the minimum ionizing track. The shower particles are mainly pions (more than 90%) having kinetic energy (K.E) > 70 MeV. They have relative velocity $\beta \geq 0.7$. Their multiplicity is denoted by n_s. The forward and backward emitted shower particles multiplicities are denoted by n_s^f and n_s^b, respectively.
— Gray particle: It is a track with range > 3 mm and $1.4g_p < g < 4.5g_p$. The gray particles consist mainly of protons knocked-out from the target nucleus. Their energy spectrum is in the range $26 <$ K.E < 400 MeV. Their multiplicity is denoted by N_g.
— Black particle: It is a track having short range ≤ 3 mm and $g \geq 4.5g_p$. These particles are mainly evaporated protons from target nuclei with K.E ≤ 26 MeV. Their multiplicity is denoted by N_b.
— The gray and black particles together amount the group of heavily ionizing target fragments, denoted by $N_h = N_g + N_b$.
— The projectile fragments are those isotopes fragmented from projectile and emitted in the narrow forward cone with θ_{lab} given by the Fermi momentum. Their rapidity is above half of the incident beam rapidity. They are identified as singly, doubly, and multiply charged nuclear clusters.

2.3. *Effective target discrimination*

The nuclear emulsion is a mixture of different nuclei. The discrimination of the effective target through a certain interaction cannot be done directly. N_h is associated with the charge of the target nucleus fragments. The interactions are classified into groups according to the target size. These groups correspond to H, CNO (the light targets), Em (the emulsion mixture as a whole), and AgBr (the heavy targets). The effective mass numbers of these target groups are 1, 14, 70, and 94, respectively. The interaction probabilities are simulated theoretically on the basis the Glauber's approach encoded in Ref. 43. They are 5.69%, 30.37%, and 63.94% according to H, CNO, and AgBr targets, respectively. The target separation method is widely explained in Ref. 44.

Table 2. Data of ^{4}He interactions in NIKFI–Br2 emulsion.

E_{lab}	L (m)	N (Events)	λ (cm)	Ref.
2.1A GeV	416.5	2066	20.2 ± 0.4	Present Work
3.7A GeV	217.6	1092	19.9 ± 0.6	
Glauber's	—	—	18.8	
3.3A GeV	—	4028	19.5 ± 0.3	45

2.4. *Interaction mean free path*

The total scanned lengths (L), the number of inelastic interaction events (N), and the measured mean free paths (λ) are listed in Table 2. The simulated mean free path according to Glauber's approach[43] is also listed in the table.

3. Results and Discussion

3.1. *Characteristics of the defined centrality factor*

The system centrality can be exactly defined but there is not an exact method to determine the centrality. In different experiments, people use different observables to determine the centrality. It depends on the impact parameter, which cannot be directly measured. It is determined by both the projectile and the target nuclear radii. Hence the selectivity of the centrality factor depends basically on the total system size. The gray particles are produced due to the binary NN collisions and/or intranuclear cascading.[46–49] The shower and gray particles have to be emitted from the participant region where the fireball nuclear matter is formed.[1,2] Therefore, the gray particle multiplicity can indicate the target nuclear matter size, binary NN collisions, and intranuclear cascading. The projectile nuclear matter size is indicated by the participant projectile proton multiplicity (Z_{part}). In this work, the centrality factor (C) can be defined from Eq. (1). The values of $\langle C \rangle$ in 2.1A and 3.7A GeV ^{4}He interactions with emulsion nuclei are listed in Table 3.

$$C = Z_{\text{part}} + N_g. \tag{1}$$

From the table, $\langle C \rangle$ increases with the target size. It decreases with the energy within standard deviation $\sim$0.25 at most. The current 2.1A GeV may still be below the onset of the nuclear limiting fragmentation. This results in the observed change

Table 3. Average centralities in 2.1A and 3.7A GeV ^{4}He interactions with emulsion nuclei.

E_{lab}	2.1A **GeV**	3.7A **GeV**
H	1.25 ± 0.08	0.92 ± 0.11
CNO	2.27 ± 0.06	1.91 ± 0.08
Em	3.98 ± 0.07	3.66 ± 0.11
AgBr	5.04 ± 0.10	4.74 ± 0.16

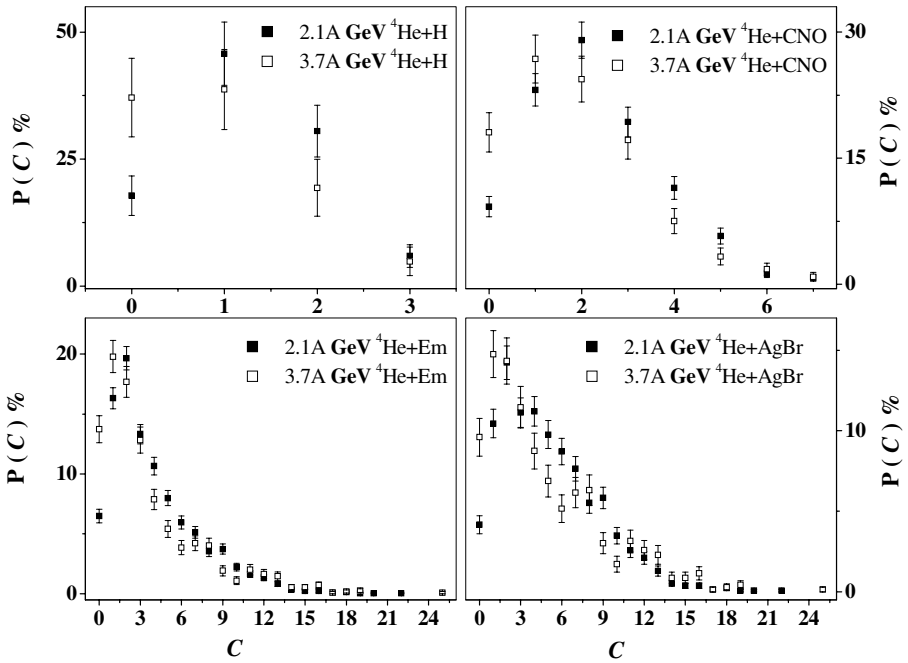

Fig. 1. Centrality distributions in 2.1A and 3.7A GeV ^{4}He interactions with emulsion nuclei.

with respect to the energy. If this change is attributed to a dependence on the energy it was supposed to be increase not decrease.

The centrality distributions for 2.1A and 3.7A GeV ^{4}He interactions with emulsion nuclei are illustrated in Fig. 1. P(C)% is the normalized centrality partition, i.e.,

$$P(C)\% = \frac{C \times 100}{\text{total no of events}}, \tag{2}$$

where $C = 0, 1, 2, \ldots, C_{\max}$. These distributions determine the percentage probability of each system centrality from the most peripheral to the most central. The peaking feature is characteristic of the distributions at all target sizes. They are nearly insensitive to the energy. The most probable centrality is at $C \sim 1$–2. It is indicated from Eq. (1) that the centrality is a superposition between the projectile and target participants. The target participants are presented by N_g. N_g-distribution is often a decay shape curve.[44,50] The possible participant protons from ^{4}He are 0, 1, or 2. Therefore, the superposition between the projectile and target participants results in the peaking shapes where the projectile contribution sustains the peak existence at $C \sim 1$–2.

3.2. *Forward emitted shower particle multiplicity characteristics at average impact parameter*

The multiplicity distributions of the forward emitted shower particle from 2.1A and 3.7A ^{4}He interactions with emulsion nuclei at average impact parameter are shown in Fig. 2. The characteristic feature of the distributions is the peaking curve shape. The distributions become broader with the target size. For light target size, H or CNO, the dependence on energy is insignificant. For larger target size the effect of the energy is reflected in the tails of the distributions. The data are fitted well by the Poisson's law, Eq. (3). α and β are fitting parameters, where α is a normalization factor and β is the average multiplicity of the forward emitted shower particle, which are listed in Table 4. For larger target size at intermediate n_s^f values the Poisson's distributions deviates from the data. This feature is due to the averaging over different impact parameters. It may also be attributed to statistical reasons. Lu *et al.*[51] suggested that the deviation from the Poisson's distribution at high multiplicity is attributed to some nonthermal process which may be responsible for pion production in extreme central collision. The β value increases with the target size and does not change significantly with the energy. The peak position shifts towards the higher multiplicity as the target size increases. The peak positions are found around the β values.

$$P(n_s^f)\% = \alpha \frac{\beta^{n_s^f}}{n_s^f!} \cdot e^{-\beta}. \tag{3}$$

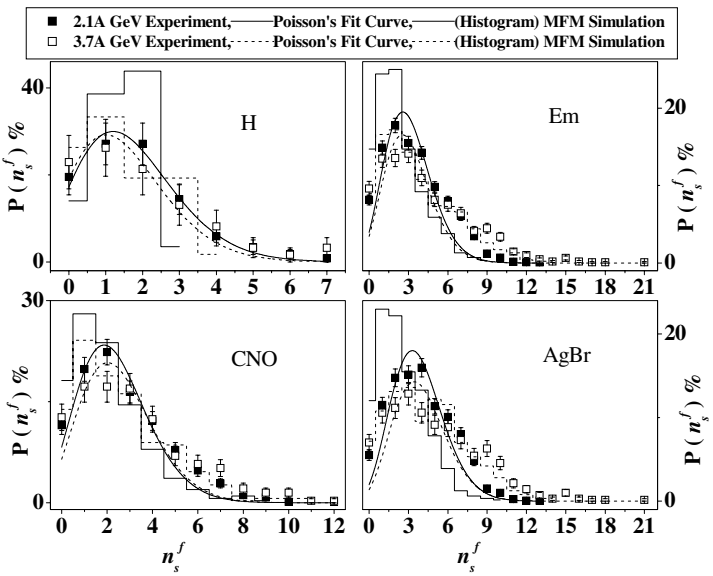

Fig. 2. Multiplicity distributions of the shower particle emitted in the FHS through 2.1A and 3.7A GeV interactions with emulsion nuclei at average impact parameter.

Table 4. Multiplicity characteristic parameters of the forward emitted shower particle in 2.1A and 3.7A GeV ^{4}He interactions with emulsion nuclei at average impact parameter.

Target	Parameter	$E_{\rm lab} = 2.1$A **GeV**	$E_{\rm lab} = 3.7$A **GeV**
H	α	96 ± 4	88 ± 7
	β	1.723 ± 0.069	1.54 ± 0.12
	χ^2/dof	0.415	1.387
	$\langle n_s^f \rangle_{\rm Exp}$	1.81 ± 0.14	1.90 ± 0.22
	$\langle n_s^f \rangle_{\rm MFM}$	1.37	1.37
	$D_{\rm Exp}$	1.478 ± 0.097	1.73 ± 0.16
	$D_{\rm MFM}$	0.760	1.11
	$D_{\rm Exp}/\langle n_s^f \rangle_{\rm Exp}$	0.82 ± 0.08	0.91 ± 0.13
	$D_{\rm MFM}/\langle n_s^f \rangle_{\rm MFM}$	0.55	0.81
CNO	α	89 ± 5	82 ± 7
	β	2.38 ± 0.11	2.54 ± 0.19
	χ^2/dof	0.339	0.706
	$\langle n_s^f \rangle_{\rm Exp}$	2.701 ± 0.081	3.10 ± 0.14
	$\langle n_s^f \rangle_{\rm MFM}$	1.964	2.57
	$D_{\rm Exp}$	2.016 ± 0.057	2.446 ± 0.095
	$D_{\rm MFM}$	1.680	2.140
	$D_{\rm Exp}/\langle n_s^f \rangle_{\rm Exp}$	0.75 ± 0.03	0.79 ± 0.05
	$D_{\rm MFM}/\langle n_s^f \rangle_{\rm MFM}$	0.86	0.83
Em	α	85 ± 6	72 ± 7
	β	3.07 ± 0.18	3.03 ± 0.24
	χ^2/dof	0.485	0.412
	$\langle n_s^f \rangle_{\rm Exp}$	3.418 ± 0.051	4.19 ± 0.10
	$\langle n_s^f \rangle_{\rm MFM}$	2.250	3.64
	$D_{\rm Exp}$	2.324 ± 0.036	3.303 ± 0.071
	$D_{\rm MFM}$	1.770	2.800
	$D_{\rm Exp}/\langle n_s^f \rangle_{\rm Exp}$	0.68 ± 0.01	0.79 ± 0.03
	$D_{\rm MFM}/\langle n_s^f \rangle_{\rm MFM}$	0.79	0.77
AgBr	α	87 ± 6	71 ± 8
	β	3.79 ± 0.19	3.94 ± 0.31
	χ^2/dof	0.419	0.028
	$\langle n_s^f \rangle_{\rm Exp}$	3.9 ± 0.1	4.91 ± 0.13
	$\langle n_s^f \rangle_{\rm MFM}$	2.5	4.36
	$D_{\rm Exp}$	2.37 ± 0.05	3.520 ± 0.094
	$D_{\rm MFM}$	1.81	2.900
	$D_{\rm Exp}/\langle n_s^f \rangle_{\rm Exp}$	0.61 ± 0.02	0.72 ± 0.03
	$D_{\rm MFM}/\langle n_s^f \rangle_{\rm MFM}$	0.72	0.67

Over a wide range of thermodynamic models Gyulassy and Kauffmann showed that the Poisson distribution can predict the emitted particle multiplicity in the central collision regions.[52] Since the used samples in Fig. 2 are unbiased to a particular centrality, then the Poisson feature suggested for central collisions[52] is also a characteristic feature of the forward emitted pion multiplicity distribution at average impact parameter. It was shown that this feature is only compatible in the few GeV region.[13,35–37,53] Above this energy ($E_{\rm lab} = 200$A GeV), the decay feature was observed.[13] In the few GeV region, the final state hadron comes from

the resonances according to the FRITIOF model assumptions. In the light of the quark–gluon string model (QGSM) the dominant sources of pions at Dubna energies are Δ and other resonances ($\rho, \omega, \eta, \eta\prime$) decay.[54] In QGSM, the pion also comes from the direct reactions. Therefore, the pion yield in this energy region is a superposition of different sources. Hence one can say that the observed Poisson's shape characteristic of the forward emitted shower particle multiplicity distribution is direct translation to the multisource superposition. On the other hand, it can be also noticed that the MFM overestimates the distributions for lower multiplicities and underestimates them for higher ones at 2.1A GeV. A qualitative agreement is observed at 3.7A GeV. Table 4 also includes the experimental and simulated average multiplicities of the forward emitted shower particle ($\langle n_s^f \rangle_{\rm Exp}$ and $\langle n_s^f \rangle_{\rm MFM}$). At 3.7A GeV, the values are qualitatively steeper than those at 2.1A GeV. They also increase with the target size. However, the target nucleus is not a source in the pionization process. The simulated values underestimate the data. On the average, the increment due to energy is nearly 1.17. Does this increment equal the ratio between the two $E_{\rm lab}$? The answer is no. Because the ratio between 3.7 and 2.1 is nearly 1.76, whereas the ratio between the equivalent values of $\sqrt{s_{NN}}$ is 1.18. In experiment[13] through the study of 3.7A and 200A GeV ^{32}S interactions with emulsion nuclei, this increment amounts nearly to 5.23. The ratio between the two $E_{\rm lab}$ (200/3.7) is nearly 54, whereas the ratio between the equivalent values of $\sqrt{s_{NN}}$ is nearly 6 which can match the result. Hence, for a certain projectile nucleus interacting with any target nucleus at two different energies, the forward emitted pion multiplicity increment due to energy nearly equals the ratio between the corresponding $\sqrt{s_{NN}}$ values.

The dispersion of the forward emitted shower particle multiplicity is defined by Eq. (4). The experimental and simulated values ($D_{\rm Exp}$ and $D_{\rm MFM}$) are listed in Table 4. They increase with energy and target size. $D_{\rm MFM}$ underestimates $D_{\rm Exp}$. The ratio $D/\langle n_s^f \rangle$ varies with the energy and target size. It was obtained in 3.7A and 200A GeV ^{32}S interactions with emulsion nuclei that $D/\langle n_s^f \rangle \sim 0.8$.[13]

$$D = \sqrt{\langle (n_s^f)^2 \rangle - \langle n_s^f \rangle^2}. \tag{4}$$

In hadron–hadron collisions, the validity of Wroblewski relation ($D = \langle n \rangle$)[55] was observed. In the light nuclear collisions under minimum bias trigger conditions, the Wroblewski relation was close to be regarded.[55] It was shown that a scaling is evident by the constancy of the ratio $\langle n \rangle / D$ at $53 \leq \sqrt{s_{NN}} \leq 900$ GeV.[56] Therefore, this ratio can be considered a scaling factor.

3.3. *Backward emitted shower particle multiplicity characteristics at average impact parameter*

The multiplicity distributions of the backward emitted shower particle from 2.1A and 3.7A GeV ^{4}He interactions with emulsion nuclei at average impact parameter are shown in Fig. 3. From the figure, the distribution belonging to the H target

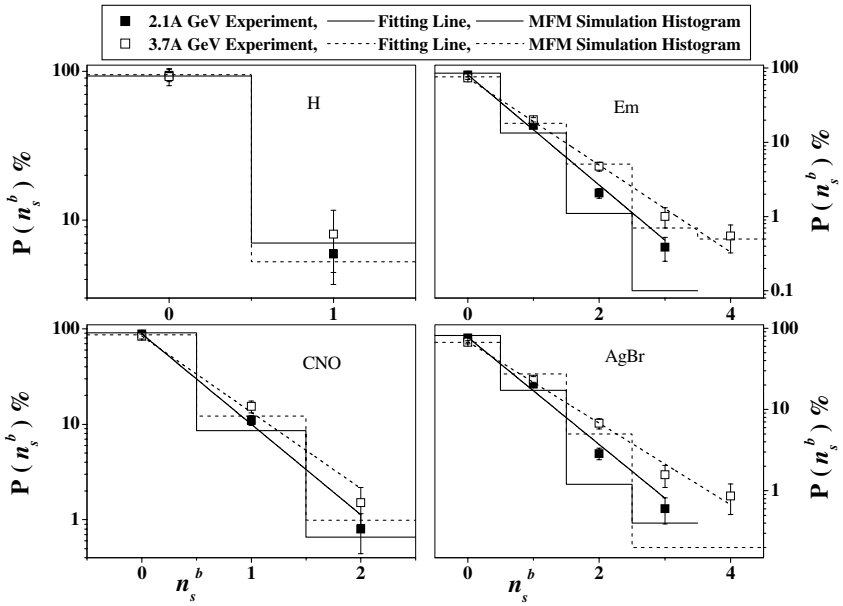

Fig. 3. Multiplicity distributions of the shower particle emitted in the BHS through 2.1A and 3.7A GeV interactions with emulsion nuclei at average impact parameter.

nuclei has no distinct feature, where it has only two data points. Since the data are presented in a semi-log frame, the characteristic feature of the distributions is the decay behavior, which is completely different from that of the forward one. The multiplicity range increases with the target size. The data are fitted well by the exponential law Eq. (5). The fitting parameters, p_s^b and λ_s^b, are listed in Table 5. The decay implies that a single source is responsible for this production system. The distributions are reproduced by the MFM.

$$P\big(n_s^b\big)\% = p_s^b e^{-\lambda_s^b n_s^b}. \tag{5}$$

From Table 5 one observes that p_s^b has a weak dependence on energy. The decay parameter (λ_s^b) at 2.1A GeV is slightly higher than that at 3.7A GeV by a factor of ∼1.2–1.3. The parameters vary with the target size. The measured and simulated average backward emitted shower particle multiplicities increase with the target size and energy. The values of $\langle n_s^b\rangle_{\rm MFM}$ often underestimate $\langle n_s^b\rangle_{\rm Exp}$. The dispersion also increases with the target size and energy. Over a wide range of projectile size, $A_{\rm proj} = 1$ up to 32, in the interactions with Em at Dubna energy a constancy of λ_s^b with respect to the projectile size was observed.[36] The average multiplicity of the backward emitted shower particle increases with the projectile size up to $A_{\rm Proj} \sim 6$. For $A_{\rm Proj} \geq 6$ saturation was observed.[36] Therefore, apart from the light nuclei, the dependence on the projectile size is insignificant in the

Table 5. Multiplicity characteristic parameters of the backward emitted shower particle in 2.1A and 3.7A GeV ^{4}He interactions with emulsion nuclei at average impact parameter.

Target	Parameter	$E_{\text{lab}} = 2.1\text{A GeV}$	$E_{\text{lab}} = 3.7\text{A GeV}$
H	$\langle n_s^b \rangle_{\text{Exp}}$	0.059 ± 0.022	0.081 ± 0.035
	$\langle n_s^b \rangle_{\text{MFM}}$	0.070	0.050
	D_{Exp}	0.236 ± 0.015	0.272 ± 0.025
CNO	p_s^b	89 ± 4	84 ± 5
	λ_s^b	2.18 ± 0.11	1.84 ± 0.12
	χ^2/dof	0.486	0.869
	$\langle n_s^b \rangle_{\text{Exp}}$	0.126 ± 0.014	0.184 ± 0.023
	$\langle n_s^b \rangle_{\text{MFM}}$	0.110	0.160
	D_{Exp}	0.355 ± 0.010	0.424 ± 0.016
Em	p_s^b	82 ± 2	74 ± 3
	λ_s^b	1.711 ± 0.042	1.352 ± 0.045
	χ^2/dof	1.580	0.201
	$\langle n_s^b \rangle_{\text{Exp}}$	0.222 ± 0.011	0.349 ± 0.020
	$\langle n_s^b \rangle_{\text{MFM}}$	0.160	0.300
	D_{Exp}	0.487 ± 0.008	0.670 ± 0.014
AgBr	p_s^b	78 ± 2	68 ± 3
	λ_s^b	1.520 ± 0.046	1.156 ± 0.048
	χ^2/dof	2.163	0.244
	$\langle n_s^b \rangle_{\text{Exp}}$	0.281 ± 0.015	0.451 ± 0.029
	$\langle n_s^b \rangle_{\text{MFM}}$	0.230	0.350
	D_{Exp}	0.544 ± 0.011	0.762 ± 0.020

backward pion production. In 3.7A and 200A GeV ^{32}S interactions with emulsion nuclei the decay parameter was constant over this wide range of energy.[13,36] It varies only with the target size. In a comprehensive study,[39] the fitting parameter (p_s^b) was nearly found 86.38, 74.36, and 65.87 for CNO, Em, and AgBr target nuclei, respectively, independent of the projectile size or energy. In the same respect, the decay parameters were nearly 2.02, 1.41, and 1.12. In the present experiment, a weak dependence on energy is observed. This may imply that, the limitation of this production system with respect to the energy at 2.1A GeV is not achieved yet. Another expectation is that ^{4}He projectile is still located before the saturation region of the limiting mechanism. Therefore, apart from the light projectiles and the lower energy region, the target size is the effective parameter in the backward pion production. This pion is suggested to result from an excited target nucleus through the de-excitation process regarding the nuclear limiting fragmentation hypothesis, while the forward emitted pion is a creation source particle.

3.4. *Scaling of shower particle multiplicity at average impact parameter*

Since the system of the backward emitted shower particle is limited with respect to the energy and projectile size, the corresponding multiplicity distribution implies a scaling law at a given target size. Otherwise the system of the forward emitted

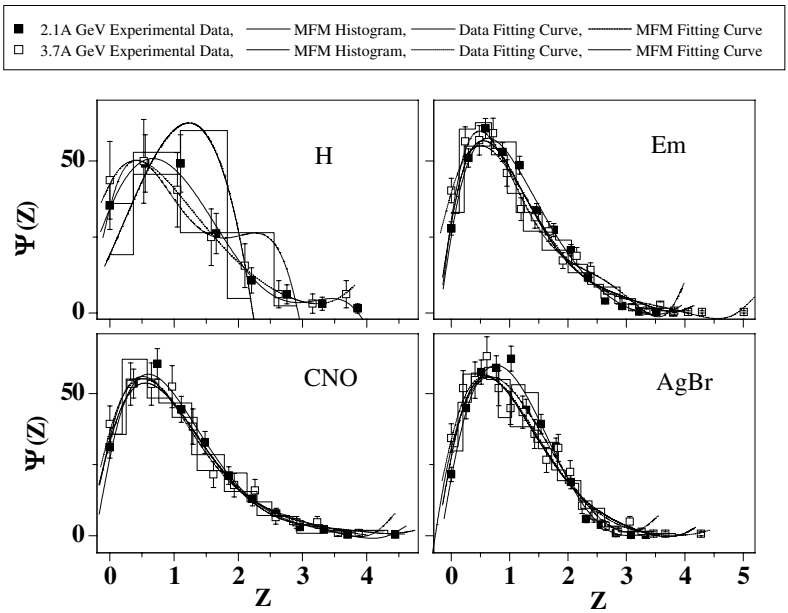

Fig. 4. KNO scaling of the forward emitted shower particle multiplicity distributions in 2.1A and 3.7A GeV ^{4}He interactions with H, CNO, Em, and AgBr emulsion nuclei at average impact parameter.

shower particle depends on the energy and system size. The KNO scaling[57] is a direct consequence of the rapidity plateau. It remains constant as the energy increases. The increase of the multiplicity comes from the stretching of the available rapidity space. Since the KNO scaling[57] is expected to hold a few GeV energies, the obtained particle multiplicity distribution was studied to test the multiplicity probability distribution. In Fig. 4, we present KNO scaling function $\psi(Z)$ of the forward emitted shower particle multiplicity distribution versus the scaling variable Z for 2.1A and 3.7A GeV ^{4}He interactions with H, CNO, Em, and AgBr at average impact parameter where,

$$Z = \frac{n_s^f}{\langle n_s^f \rangle}, \tag{6}$$

$$\psi(Z) = \langle n_s^f \rangle P(n_s^f). \tag{7}$$

As observed, the data show energy independence. A scaling validity is indicated. The MFM simulation agrees with the scaled distributions, except for H target. The data and simulations are approximated well by a fifth-order polynomial Eq. (8). The fitting parameters (a_i) are presented against A_T in Fig. 5 to show the dependence on the target size.

$$\psi(Z) = \sum_{i=0}^{5} a_i Z^{\mathrm{i}}. \tag{8}$$

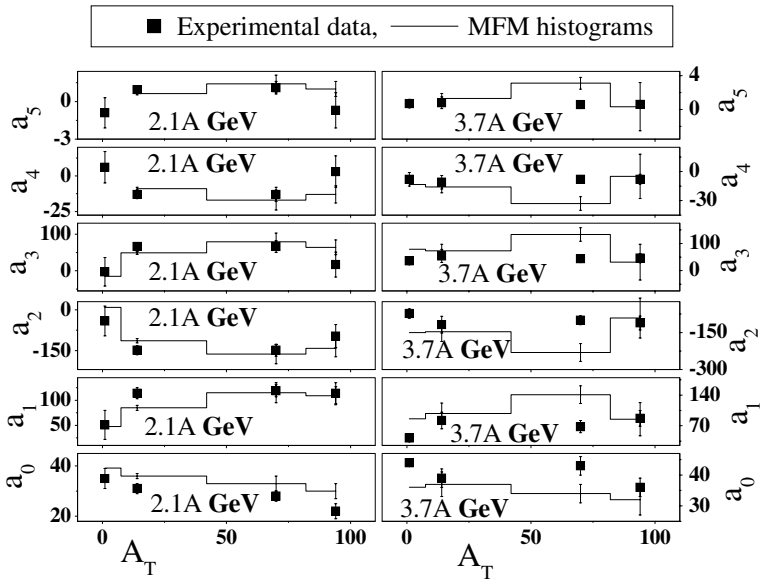

Fig. 5. Dependence of Eq. (8) fitting parameters on the target size.

3.5. *Shower particle multiplicity correlation at average impact parameter*

Figure 6 shows the dependence of the average forward emitted shower particle multiplicity on the backward emitted shower particle multiplicity in 2.1A and 3.7A GeV ^{4}He interactions with emulsion nuclei at average impact parameter. $\langle n_s^f \rangle$ increases linearly with n_s^b. The fitting parameters characterizing the line segments are listed in Table 6. This correlation does not mean that the forward and backward emitted shower particles come from the same origin, but they increase with the centrality. The intercepts (at $n_s^b = 0$) are compatible within experimental error at the two energies. The intercept increases slowly with the target size. The slope changes with the target size and energy. At 3.7A GeV the slope parameter is (2 to 4.5) times that at 2.1A GeV.

3.6. *Forward emitted shower particle multiplicity distributions at different centralities*

The forward emitted shower particle multiplicity distributions of 2.1A and 3.7A GeV ^{4}He interactions with CNO and AgBr emulsion nuclei are presented at different centralities in Fig. 7. The peaking shaped curves are a characteristic of the distributions. The peak often shifts forward with the energy and centrality. The distributions are well fitted by the Poisson's law Eq. (3). They shift from the shoulder shape at $C = 0$ to semi-bell shape at higher centralities. They are about to be symmetric at $C > 3$. The symmetry implies a similarity to the Gaussian shape

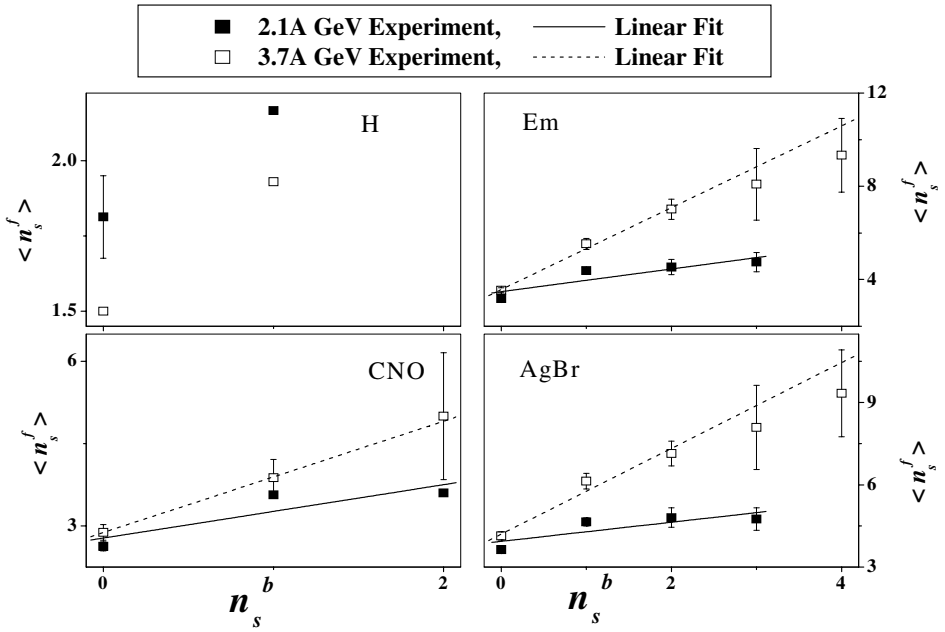

Fig. 6. Dependence of the average forward emitted shower particle multiplicity on the backward emitted one in 2.1A and 3.7A GeV ^{4}He interactions with H, CNO, Em, and AgBr emulsion nuclei at average impact parameter.

Table 6. Fit parameters of the straight line segments shown in Fig. 6.

Target	Fitting parameter	$E_{\text{lab}} = 2.1\text{A GeV}$	$E_{\text{lab}} = 3.7\text{A GeV}$
CNO	Intercept	2.78 ± 0.34	2.880 ± 0.013
	Slope	0.49 ± 0.26	1.016 ± 0.028
	χ^2/dof	0.021	0.001
Em	Intercept	3.48 ± 0.33	3.575 ± 0.077
	Slope	0.49 ± 0.17	1.76 ± 0.12
	χ^2/dof	0.026	0.057
AgBr	Intercept	3.94 ± 0.33	4.20 ± 0.14
	Slope	0.35 ± 0.17	1.56 ± 0.17
	χ^2/dof	0.023	0.056

associated with an isotropy of state. In this state, the contributions of the multi sources to the production system are equivalent. Hence, in the most central case the multisource superposition is isotropic.

3.7. *Backward emitted shower particle multiplicity distributions at different centralities*

The backward emitted shower particle multiplicity distributions at different centralities of 2.1A and 3.7A GeV ^{4}He interactions with CNO emulsion nuclei are

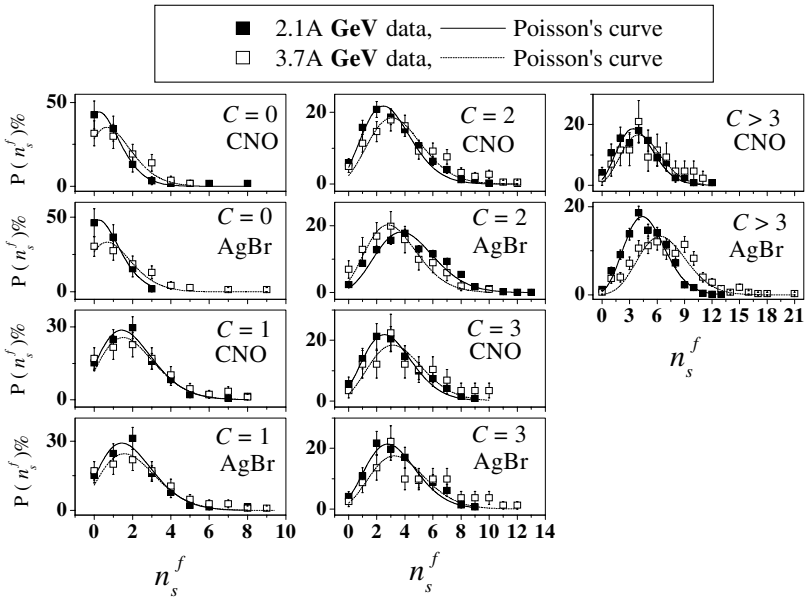

Fig. 7. Multiplicity distributions of the forward emitted shower particle at different centralities of 2.1A and 3.7A GeV ^{4}He interactions with CNO and AgBr emulsion nuclei.

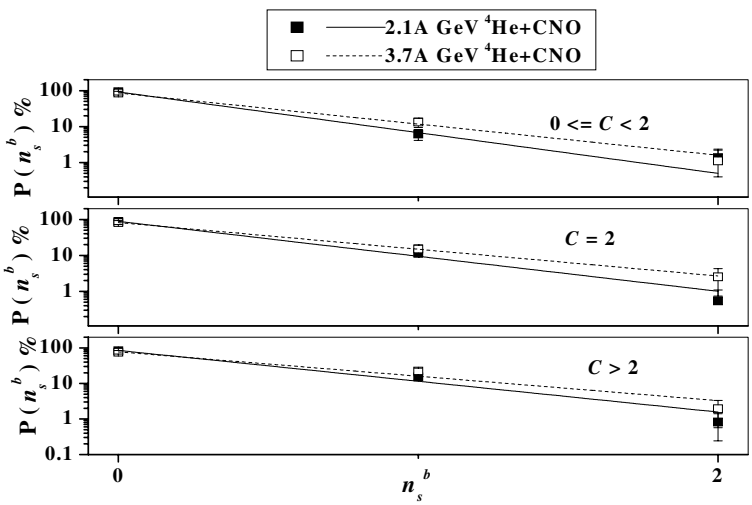

Fig. 8. Multiplicity distributions of the backward emitted shower particle at different centralities of 2.1A and 3.7A GeV ^{4}He interactions with CNO emulsion nuclei.

displayed in Fig. 8. The distributions are usually characterized by a decay shape. This indicates a single source responsible for the production at all centralities. The distributions are approximated by an exponential law Eq. (5). The corresponding fitting parameters are listed in Table 7. The decrement rate of p_s^b due to the

Table 7. Fitting parameters of the curves shown in Fig. 8.

Fitting parameter	p_s^b		λ_s^b		χ^2/dof	
E_{lab}	2.1A **GeV**	3.7A **GeV**	2.1A **GeV**	3.7A **GeV**	2.1A **GeV**	3.7A **GeV**
$0 \leq C < 2$	92 ± 8	86 ± 10	2.61 ± 0.30	1.99 ± 0.25	0.446	0.184
$C = 2$	89 ± 7	82 ± 10	2.24 ± 0.20	1.71 ± 0.24	0.698	0.006
$C > 2$	85 ± 6	78 ± 8	2.00 ± 0.15	1.58 ± 0.18	1.934	1.436

centrality or energy is (3–5%) or (7–9%), respectively. In the same respect, the decrement rate of λ_s^b is (8–17%) or (27–31%). Therefore, in ^{4}He+CNO collisions, the pion production beyond the kinematic limit weakly depends on the energy and centrality. However, the dependence on the centrality is weaker than the energy.

The backward emitted shower particle multiplicity distributions at different centralities for 2.1A and 3.7A GeV ^{4}He interactions with AgBr emulsion nuclei are displayed in Fig. 9. From Fig. 9, the distributions are approximated by Eq. (5) up to $C = 3$. The corresponding fitting parameters are listed in Table 8. A single source of this production is indicated by the decay behavior in the peripheral region. The decrement rate of p_s^b due to the centrality or energy is (0–9%) or (7–14%), respectively. In the same respect, the decrement rate of λ_s^b is (3–25%) or (33–43%). The dependence on the centrality seems to be weak, whereas on the energy the effect is considerable. At $C > 3$ the distributions are shoulder shaped curves. They are well approximated by the Poisson's law Eq. (3), which indicates a multisource superposition. Since the distributions cannot have the Gaussian bell shapes, the isotropy of

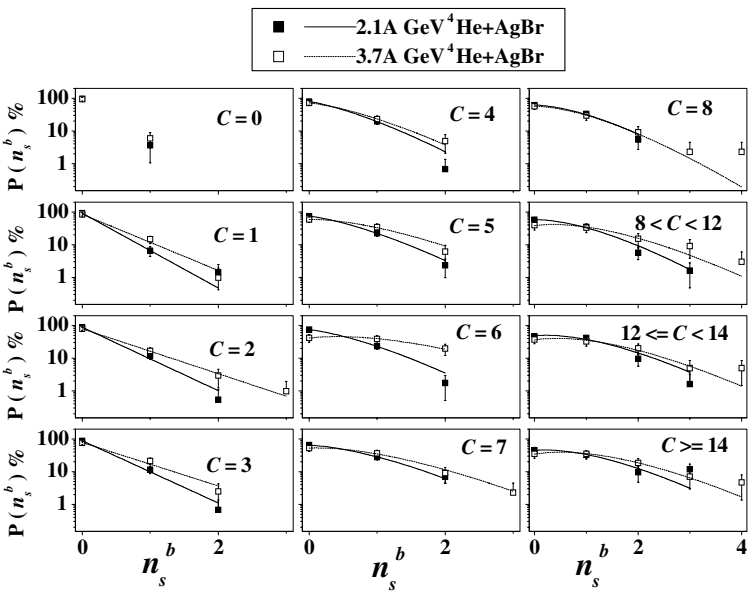

Fig. 9. Multiplicity distributions of the backward emitted shower particle at different centralities of 2.1A and 3.7A GeV ^{4}He interactions with AgBr emulsion nuclei.

Table 8. Fitting parameters of the exponential decay curves shown in Fig. 9.

Fitting parameter	p_s^b		λ_s^b		χ^2/dof	
E_{lab}	2.1A **GeV**	3.7A **GeV**	2.1A **GeV**	3.7A **GeV**	2.1A **GeV**	3.7A **GeV**
$C = 1$	92 ± 1	86 ± 9	2.63 ± 0.15	1.98 ± 0.23	0.474	0.506
$C = 2$	89 ± 7	79 ± 9	2.23 ± 0.20	1.58 ± 0.18	0.825	0.026
$C = 3$	89 ± 8	78 ± 10	2.19 ± 0.22	1.53 ± 0.21	0.369	0.588

state does not exist, where the contribution of the sources is not equivalent. Hence, the target size plays an important role. This confirms that the backward emitted pion is a target source particle.[13,33,36–39,58] One of the suggested sources is the nuclear cluster decay in the cumulative region.[59–62] The other one is based on the effective target model[63] by Schroeder *et al.*,[10] in which the backward emitted pion is produced due to the dominance of a single NN scattering in peripheral region at $E_{lab} \leq 3$ GeV.

3.8. *Shower particles average multiplicities at different centralities*

The dependence of the forward and backward emitted shower particles average multiplicities on the centrality through 2.1A and 3.7A GeV ^{4}He interactions with H, CNO, and AgBr emulsion nuclei is presented in Fig. 10. The average multiplicities (β) obtained by the Poisson's fitting are presented in Fig. 10. At $\theta_{lab} < 90°$, the intercept difference between the two energies is within (7–29%) and the slope difference is within (1–5%). In ^{4}He+H collisions, the dependence is approximately linear along the centrality range. In ^{4}He+CNO collisions, the linear approximation is carried out up to $C = 2$, beyond which saturation is observed. In the saturation region $\langle n_s^f \rangle$ is limited to ∼3.5. In ^{4}He+AgBr collisions, the linear approximation is carried out up to $C = 4$. At $C > 4$ saturation exists. In the saturation region $\langle n_s^f \rangle$ is limited to ∼5. It seems β value does not deviate at higher centralities for lighter target. It only deviates for heavier targets. On the other hand, $\langle n_s^b \rangle$ depends linearly on the centrality. The slope difference between the two energies is within (17–57%).

The dependence of the ratio, $D/\langle n_s^f \rangle$, on the centrality through 2.1A and 3.7A GeV ^{4}He interactions with H, CNO, and AgBr emulsion nuclei is shown in Fig. 11. A linear decrease or inverse allometric approximation is performed with fitting parameters listed in Table 9. The allometric approximation is determined by Eq. (9), where a and b are the fitting parameters.

$$D/\langle n_s^f \rangle = aC^b. \tag{9}$$

The decrease reflects the dominance of the impact parameter variation over the hadronization fluctuations at different energies. In ^{4}He+H collisions, the dependence is nearly the same at the two energies where the standard deviation between the fitting parameters ∼0.004 and 0.005 for the intercept and slope, respectively. In

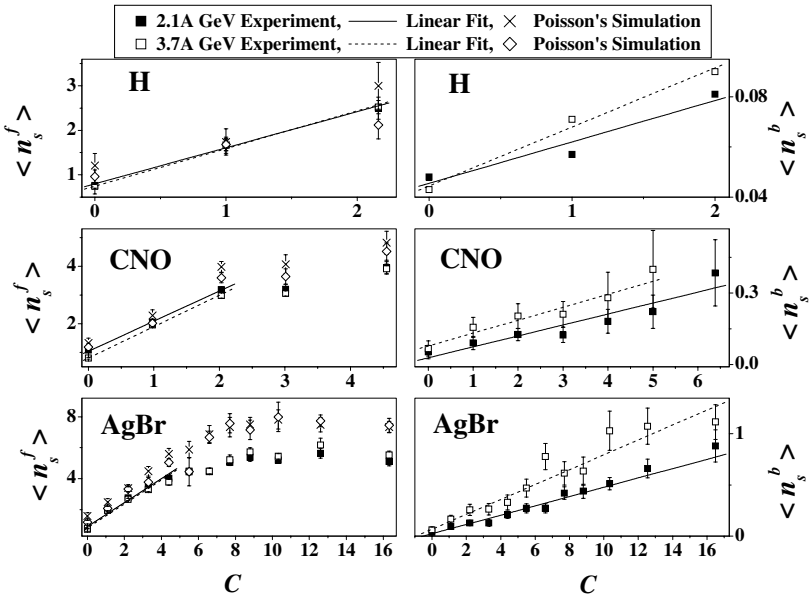

Fig. 10. Dependence of the average forward and backward emitted shower particles multiplicities on the centrality through 2.1A and 3.7A GeV ^{4}He interactions with H, CNO, and AgBr emulsion nuclei.

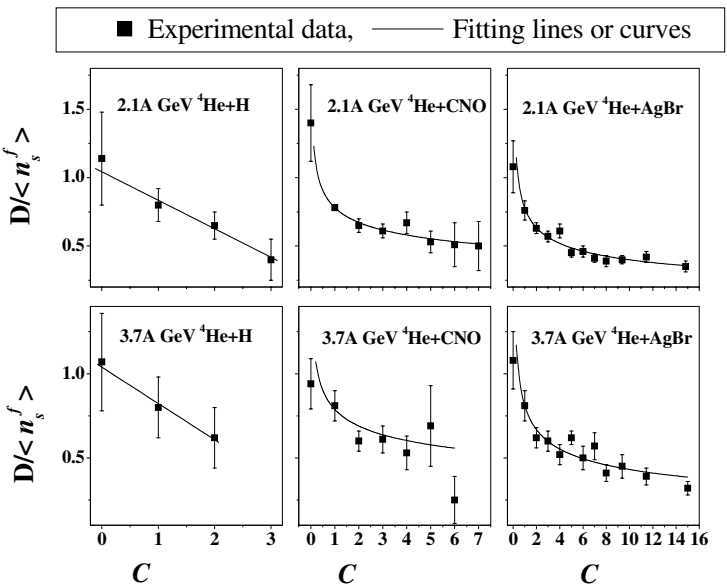

Fig. 11. Dependence of $D/\langle n_s^f \rangle$ on the centrality in 2.1A and 3.7A GeV ^{4}He interactions with H, CNO, and AgBr emulsion nuclei.

Table 9. Fitting parameters of the line segments and curves shown in Fig. 11.

Target	Fitting parameter	$E_{\text{lab}} = 2.1\text{A GeV}$	Fitting parameter	$E_{\text{lab}} = 3.7\text{A GeV}$
H	Intercept	1.044 ± 0.057	Intercept	1.039 ± 0.042
	Slope	-0.209 ± 0.029	Slope	-0.216 ± 0.029
CNO	a	0.78 ± 0.04	a	0.79 ± 0.15
	b	-0.21 ± 0.04	b	-0.19 ± 0.17
AgBr	a	0.77 ± 0.03	a	0.81 ± 0.05
	b	-0.29 ± 0.03	b	-0.27 ± 0.04

^{4}He+CNO collisions, the standard deviation is $\sim$0.007 and 0.01 for a and b, respectively. For the same respect in ^{4}He+AgBr collisions, the standard deviation is $\sim$0.03 and 0.01. Hence, the independence on the energy can exist. The linear dependence may be associated with a short centrality range. The allometric dependence is associated with wide centrality range over which the scaling ratio is asymptotic at higher centralities.

4. Summary

Measurements of the shower particle multiplicity in 2.1A and 3.7A GeV ^{4}He interactions with emulsion nuclei provide a good insight into the pion production mechanisms. The multiplicity is determined in terms of the energy, emission zone, target size, and centrality.

(1) The mean free path of ^{4}He in NIKFI–BR2 emulsion type is measured and simulated by the Glauber's approach to be ($\sim$19 to 20 cm). It is independent on the energy.

(2) The defined centrality parameter distribution is always a peak shaped curve. The peak positions are located at $C \sim 1$–2, showing the bulk of the interactions takes place in the peripheral region.

(3) The forward emitted shower particle multiplicity distributions are always characterized by peaking feature at few GeV, independent of the impact parameter or system size. The Poisson distribution fits the data reasonably well. The multiplicity distributions are broader with increasing energy, target size, and centrality, where the multiplicity range becomes wider. The peak position moves forward with the centrality from the most peripheral to the most central region. The curves change with the centrality from shoulder to bell shapes. The peaking feature of the distribution suggests a multisource superposition. At any centrality channel having $C > 3$ the distributions become nearly symmetric about the peak. They look like Gaussian shapes as the multisource superposition is expected to be isotropic in the most central region.

(4) In principle, the results indicate that the forward emitted pion is sourced from a fireball of nuclear matter or hadronic matter.

(5) The forward emitted shower particle average multiplicity increases with the energy and system size. On the average, the increment due to the energy amounts nearly to 1.17, which can match the ratio between the equivalent values of $\sqrt{s_{NN}}$.

In ^{4}He+H collision $\langle n_s^f \rangle$ increases linearly with the centrality. In ^{4}He+CNO and ^{4}He+AgBr collisions, the linearity continues up to $C = 2$ and 4, respectively. At higher centralities saturations are observed. In the same respect $\langle n_s^f \rangle$ tends to 3.5 and 5 at the saturation regions. The average multiplicity is fitted satisfactorily by the Poisson's law.

(6) The decrease of the ratio $(D/\langle n_s^f \rangle)$ with the centrality implies the dominance of the impact parameter in the hadronization fluctuations at different energies.

(7) The forward emitted shower particle multiplicity distributions at average impact parameters exhibit KNO scaling. The scaling law can be determined by a fifth-order polynomial.

(8) The backward emitted shower particle multiplicity distributions are usually characterized by a decay shape at average impact parameters, at all centralities of ^{4}He+CNO collisions, and in peripheral ^{4}He+AgBr collisions. They are approximated by an exponential law. The fitting parameters are weakly dependent on the centrality, whereas the effect of energy is qualitatively considerable. At $C > 3$ of ^{4}He+AgBr collisions, the distributions are shoulder shaped presented by Poisson's curves. This implies that there is more than one source contributes to the distributions. One source is suggested in the cumulative phenomena,[59–62] where the pion is a decay of nuclear cluster. The second is expected on the basis of the effective target model[10,63] to be dominant in the peripheral collisions at $E_{\rm lab} \leq 3$ GeV. Since the usual characteristic at the average impact parameters is the decay shape, hence one of the two suggested sources is dominant. Although the nuclear limiting fragmentation was regarded in this production system,[13,33,36–39,58] a dependence on the energy is observed. This implies that ($E_{\rm lab} = 2.1A$ GeV) and ^{4}He projectile still before the onset of the nuclear limiting fragmentation for this production. This agrees with the suggestion of Schroeder *et al.*,[10] in which the onset of the limiting fragmentation for this production system is nearly within 3 to 4 GeV.

(9) The backward emitted shower particle average multiplicity has always a linear dependence on the centrality. The forward emitted shower particle average multiplicity is correlated linearly with the backward emitted one.

(10) The MFM simulation reproduces qualitatively the backward emitted pion multiplicity distributions. In general, the MFM simulations overestimate the forward emitted shower particle multiplicity distributions. They underestimate the average multiplicities and dispersions. The MFM simulation deviates from the KNO scaling validity in collisions with H. Meanwhile it scales for the other target nuclei data.

5. Main Conclusion

— The forward emitted pion is created from fireball of nuclear matter or hadronic matter. Multisource contributes to this production system at few GeV.

— The backward emitted pion is a target source particle, where the nuclear limiting fragmentation hypothesis is well regarded. Two sources are suggested to

contribute to this production system. However, one of the two suggested sources is more dominant.

— The decay-shaped distribution presents the single source contribution and the peaking one is multisource superposition. The source contribution depends on the energy, system size, centrality, and emission zone.

Acknowledgment

We would like to acknowledge the great help of JINR, Dubna, Russia, specially Vekseler and Baldin High Energy Laboratory for supplying us the photographic emulsion plates. The authors appreciate the valuable helps of Prof. M. K. Hegab and Prof. Ali Ellithi, faculty of science, Cairo university.

References

1. G. D. Westfall, J. Gosset, P. J. Johansen, A. M. Poskanzer, W. G. Meyer, H. H. Gutbrod, A. Sandoval and R. Stock, *Phys. Rev. Lett.* **37** (1976) 1202.
2. J. Gosset, H. H. Gutbrod, W. G. Meyer, A. M. Poskanzer, A. Sandoval, R. Stock and G. D. Westfall, *Phys. Rev. C* **16** (1977) 629.
3. B. Andersson, G. Gustafson, G. Ingelman and T. Sjöstrand, *Phys. Rep.* **97** (1983) 31.
4. B. Nilsson-Almqvist and E. Stenlund, *Comp. Phys. Comm.* **43** (1987) 387.
5. B. Andersson, G. Gustafson and B. Nilsson-Almqvist, *Nucl. Phys. B* **281** (1987) 289.
6. M. I. Adamovich *et al.* for EMU01 Collab., *Z. Phys. A* **358** (1997) 337.
7. A. M. Baldin, *Yad. Fiz.* **10** (1971) 1201.
8. A. M. Baldin, N. Giordenescu, V. N. Zubarev, L. K. Ivanova, N. S. Moroz, A. A. Povtoreĭko, V. B. Radomanov and Stavinskiĭ, *Sov. J. Nucl. Phys.* **20** (1975) 629.
9. S. Fredriksson, *Phys. Rev. Lett.* **45** (1980) 1371.
10. L. S. Schroeder, S. A. Chessin, J. V. Geaga, J. Y. Grossiord, J. W. Harris, D. L. Hendrie, R. Treuhaft and K. Van Bibber, *Phys. Rev. Lett.* **43** (1979) 1787.
11. J. V. Geaga, S. A. Chessin, J. Y. Grossiord, J. W. Harris, D. L. Hendrie, L. S. Schroeder, R. N. Treuhaft and K. Van Bibber, *Phys. Rev. Lett.* **45** (1980) 1993.
12. M. El-Nadi, A. Abdelsalam, N. Ali-Mossa, Z. Abou-Moussa, Kh. Abdel-Waged, W. Osman and B. M. Badawy, *IL Nuovo Cimento A* **111** (1998) 1243.
13. A. Abdelsalam, B. M. Badawy and M. Hafiz, *J. Phys. G: Nucl. Part. Phys.* **39** (2012) 105104.
14. V. Uzhinsky, Development of the Fritiof Model in Geant4, *Joint International Conf. on Supercomputing in Nuclear Applications and Monte Carlo 2010* (*SNA + MC 2010*), Hitotsubashi Memorial Hall, Tokyo, Japan, 17–21 October 2010.
15. K. Abdel-Waged and V. V. Uzhinsky, *Phys. Atom. Nucl.* **60** (1997) 828; *Yad. Fiz.* **60** (1997) 925.
16. K. Abdel-Waged and V. V. Uzhinsky, *J. Phys. G: Nucl. Part. Phys.* **24** (1997) 1723.
17. M. El-Nadi, A. Abdel Salam, A. Hussein, E. A. Shaat, N. Ali-Mousa, Z. Abou-Mousa, S. Kamel, Kh. Abdel-Waged and E. El-Falaky, *Int. J. Mod. Phys. E* **6** (1997) 191.
18. K. Aamodt *et al.* ALICE Collab., *Eur. Phys. J. C* **71** (2011) 1655.
19. J. Adam *et al.* ALICE Collab., *Eur. Phys. J. C* **75** (2015) 226.
20. S. S. Adler *et al.* PHENIX Collab., *Phys. Rev. Lett.* **91** (2003) 072301.
21. S. C. Johnson for PHENIX, *Nucl. Phys. A* **698** (2002) 603.
22. S. S. Adler *et al.* PHENIX Collab., *Phys. Rev. Lett.* **93** (2004) 152302.
23. I. C. Arsene *et al.* BRAHMS Collab., *Phys. Lett. B* **687** (2010) 36.

24. B. I. Abelev STAR Collab., *Phys. Rev. C* **80** (2009) 044905.
25. A. Kocoloski STAR Collab., *AIP Conf. Proc.* **1149** (2009) 277.
26. J. Adams *et al.* STAR Collab., *Phys. Rev. Lett.* **97** (2006) 152302.
27. L. Adamczyk *et al.* for STAR Collab., *Phys. Rev. C* **96** (2017) 044904.
28. M. El-Nadi, N. Ali-Mossa and A. Abedelsalam, *Int. J. Mod. Phys. E* **3** (1994) 811.
29. M. El-Nadi, A. Abedelsalam and N. Ali-Moussa, *Radiat. Phys. Chem.* **47** (1996) 681.
30. M. El-Nadi M, N. Ali-Mossa and A. Abedelsalam, *IL Nuovo Cimento A* **110** (1998) 1255.
31. K. Abdel-Waged, *Phys. Rev. C* **59** (1999) 2792.
32. K. Abdel-Waged, *J. Phys. G: Nucl. Part. Phys.* **25** (1999) 1721.
33. A. Abdelsalam, E. A. Shaat, N. Ali-Mossa, Z. Abou-Mousa, O. M. Osman, N. Rashed, W. Osman, B. M. Badawy and E. El-Falaky, *J. Phys. G: Nucl. Part. Phys.* **28** (2002) 1375.
34. A. Abdelsalam, B. M. Badawy and E. El-Falaky, *Can. J. Phys.* **85** (2007) 837.
35. B. M. Badawy, *Int. J. Mod. Phys. E* **18** (2009) 648.
36. A. Abdelsalam, M. S. El–Nagdy and B. M. Badawy, *Can. J. Phys.* **89** (2011) 261.
37. A. Abdelsalam, B. M. Badawy and M. Hafiz, *Can. J. Phys.* **90** (2012) 515.
38. A. Abdelsalam, E. A. Shaat, Z. Abou-Moussa, B. M. Badawy and Z. S. Mater, *Chin. Phys. C* **37** (2013) 084001.
39. B. M. Badawy, *Chin. Phys. C* **38** (2014) 114001.
40. M. I. Adamovich EMU01 Collab., *J. Phys. G*: *Nucl. Part. Phys.* **22** (1996) 1469.
41. C. F. Powell, F. H. Fowler and D. H. Perkins, *The Study of Elementary Particles by the Photographic Method* (Pergamon Press. London, New York, Paris, Los Angles, 1958). p. 474.
42. H. Barkas, *Nuclear Research Emulsion*, Vol. I (Technique and Theory Academic Press Inc., 1963).
43. S. Yu. Shmakov and V. V. Uzhinskii, *Com. Phys. Comm.* **54** (1989) 125.
44. A. Abdelsalam, M. S. El–Nagdy, B. M. Badawy, W. Osman and M. Fayed, *Int. J. Mod. Phys. E* **25** (2016) 1650034.
45. G. S. Shabratova *et al.*, *Acta Phys. Slov.* **28** (1978) 132.
46. V. I. Bubnov *et al.*, *Z. Phys. A* **302** (1981) 133.
47. M. K. Hegab and J. Hüfner, *Phys. Lett. B* **105** (1981) 103.
48. M. K. Hegab and J. Hüfner, *Nucl. Phys. A* **384** (1982) 353.
49. M. Tosson, O. M. Osman, M. M. Osman and M. K. Hegab, *Z. Phys. A* **347** (1994) 247.
50. A. Abdelsalam, M. S. El-Nagdy, N. Rashed, B. M. Badawy, W. Osman and M. Fayed, *Can. J. Phys.* **93** (2015) 361.
51. J. J. Lu, D. Beavis, S. Y. Fung, W. Gorn, A. Huie, G. P. Kiernan, R. T. Poe and G. Van Dalen, *Phys. Rev. Lett.* **46** (1981) 898.
52. M. Gyulassy and S. K. Kauffmann, *Phys. Rev. Lett.* **40** (1978) 298.
53. M.-C. Lemaire *et al.*, *Phys. Rev. C* **43** (1991) 2711.
54. S. Backović, D. Salihagić, Lj. Simić, D. Krpić, S. Drndarević, R. R. Mekhdiyev, A. P. Cheplakov, H. N. Agakishiev, E. N. Kladnitskaya and S. Yu. Sivoklokov, *Phys. Rev. C* **46** (1992) 1501.
55. R. Stock, *Phys. Rep.* **135** (1986) 259.
56. J. F. Sagerer, Proton proton multiplicity distributions at the relativistic heavy ion collider, A Thesis submitted in partial fulfillment of the requirements for the degree of Doctor of Philosophy in physics in the Graduate College of the University of Illinois at Chicago in 2008.
57. Z. Koba, H. B. Nielsen and P. Olesen, *Nucl. Phys. B* **40** (1972) 317.

58. A. Abdelsalam, Z. Abou-Moussa, N. Rashed, B. M. Badawy, H. A. Amer, W. Osman, M. M. El-Ashmawy and N. Abdallah, *Chin. Phys. C* **39** (2015) 094001.
59. A. M. Baldin, *Part. Nucl.* **8** (1977) 429.
60. M. I. Gorenstein and G. M. Zinovjev, *Phys. Lett. B* **67** (1977) 100.
61. M. I. Gorenstein, V. P. Shelest and G. M. Zinovjev, *Yad. Fiz.* **26** (1977) 788 [*Sov. J. Nucl. Phys.* **26** (1977) 414].
62. I. G. Bogatskaya, C. B. Chiu, M. I. Gorenstein and G. M. Zinovjev, *Phys. Rev. C* **22** (1980) 209.
63. H. B. Mathis and Meng Ta-Chung, *Phys. Rev. C* **18** (1978) 952.